Jason Melidonie, Junzhi Liu, Yubin Fu, Jan J. Weigand, Reinhard Berger, Xinliang Feng

Pyrene-Fused s-Indacene

Erstveröffentlichung in / First published in:

The Journal of Organic Chemistry. 2018, 139 (48), S. 6633 – 6639. ACS Publications. ISSN 1520-6904.

DOI: https://doi.org/10.1021/acs.joc.8b00925

JOC The Journal of Organic Chemistry
Cite This: J. Org. Chem. 2018, 83, 6633−6639
Article
pubs.acs.org/joc

Pyrene-Fused *s*-Indacene

Jason Melidonie,[†] Junzhi Liu,[†] Yubin Fu,[†] Jan J. Weigand,[‡] Reinhard Berger,*[,†] and Xinliang Feng*[,†]

[†]Center for Advancing Electronics Dresden (cfaed) and Faculty of Chemistry and Food Chemistry and [‡]Chair of Inorganic Molecular Chemistry, Technische Universität Dresden, 01062 Dresden, Germany

Supporting Information

ABSTRACT: One antiaromatic polycyclic hydrocarbon (PH) with and without solubilizing *tert*-butyl substituents, namely *s*-indaceno[2,1-*a*:6,5-*a*′]dipyrene (IDPs), has been synthesized by a four-step protocol. The IDPs represent the longitudinal, *peri*-extension of the indeno[1,2-*b*]fluorene skeleton towards a planar 40 π-electron system. Their structures were unambiguously confirmed by X-ray crystallographic analysis. The optoelectronic properties were studied by UV/vis absorption spectroscopy and cyclic voltammetry. These studies revealed that *peri*-fusion renders the IDP derivatives with a narrow optical energy gap of 1.8 eV. The maximum absorption of IDPs is shifted by 160 nm compared to the parent indenofluorene. Two quasi-reversible oxidation as well as reduction steps indicate an excellent redox behavior attributed to the antiaromatic core. Formation of the radical cation and the dication was monitored by UV/vis absorption spectroscopy during titration experiments. Notably, the fusion of *s*-indacene with two pyrene moieties lead to IDPs with absorption maxima approaching the near infrared (NIR) regime.

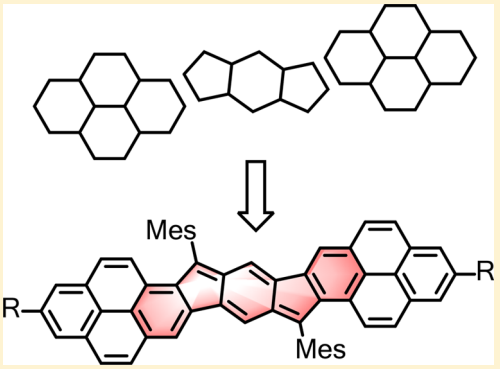

INTRODUCTION

Polycyclic hydrocarbons (PHs) featuring antiaromaticity have been in the focus of research for decades because of their unique electronic structure and the related magnetic, photophysical, and electronic properties.[1] In contrast to polycyclic aromatic hydrocarbons (PAHs), their absorption maxima are significantly bathochromic shifted, as the energy difference of their frontier orbitals is significantly reduced and comparable to those of the acene series.[2] The narrow optical energy gap renders antiaromatic PHs promising materials for application in optoelectronic devices.[3,4] The most common way to obtain antiaromatic, π-conjugated structures is embedding a *s*-indacene moiety into the core of a π-conjugated framework, in which a quinodimethane (QDM) subunit is found.[5] This strategy has been widely used to synthesize antiaromatic but also proaromatic PHs with partial diradical character.[6] Several *ortho*-,[7] *meta*-,[8] and *para*-QDM[9] structures have been synthesized in the past years by Wu, Tobe, and Haley whereby *m*- and *o*-structures are considered as highly reactive due to their increased open-shell character compared to their *p*-analogues. Typical *p*-QDM representatives are diphenalenes[10] and octazethrenes,[11] which feature a biradical character up to 0.68,[12] as well as indeno[1,2-*b*]fluorenes (IF, red substructures in the formula displayed in Figure 1)[2] which can be regarded as benzo-fused *s*-indacenes with an usually insignificant biradical character.[13] Therefore, IFs are considered as stable closed-shell systems. Moreover, indeno[1,2-*b*]fluorene shows notable resistance toward air, light, and heat when protective substituents, such as mesityl (Mes), at the reactive 6- and 12-positions are introduced.[14]

The stability enables processability for potential application in organic field-effect transistors (OFETs), photovoltaics (OPVs), and light-emitting diodes (OLEDs).[15−17] To further tune their optoelectronic properties, several longitudinal extended indenofluorenes have been synthesized by Haley. As exemplified in Figure 1, in these derivatives, the benzene rings for **2a**−**2d**[18] and also heteroatom containing analogs are fused in *ortho*-fashion to the parent IF.[19−21] Recently, our group also reported lateral *ortho-peri* - along the "bay-position" -extended indeno[1,2-*b*]fluorenes **3a** and **3b**, resulting in twisted geometries.[22] In contrast to *ortho*- (**2a**−**2d**) and *ortho-peri*-expansion (**3a** and **3b**), whereby conjugation is extended only over two bonds (indicated by the dashed bonds in Figure 1), *peri*-fusion of PAHs extends the conjugation along three directions, and thus, a significant effect on the optoelectronic properties is expected.[9]

RESULTS AND DISCUSSION

In this work, we report a scalable four-step synthetic route to *s*-indacenodipyrenes (IDPs), namely 8,18-dimesityl-*s*-indaceno-[2,1-*a*:6,5-*a*′]dipyrene (**1a**) and 2,12-di-*tert*-butyl-8,18-dimesityl-*s*-indaceno[2,1-*a*:6,5-*a*′]dipyrene (**1b**). Formal *peri*-fusion causes a red shift of ∼160 nm of the maximum absorption from 512 nm for the parent IF to 676 nm for **1a** and 682 nm (**1b**), thus approaching the NIR region.[14]

Received: April 12, 2018
Published: May 18, 2018

DOI: 10.1021/acs.joc.8b00925
J. Org. Chem. 2018, 83, 6633−6639

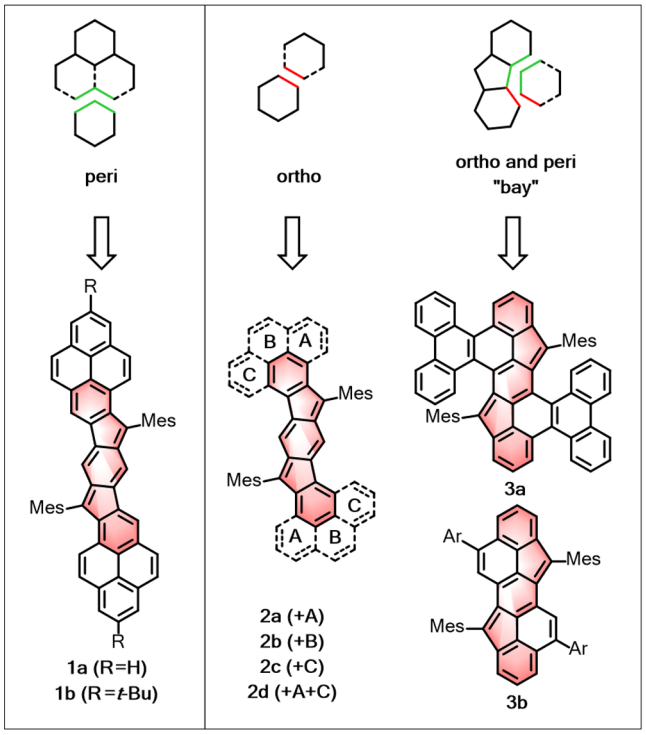

Figure 1. Representation of the different fusion-patterns for IF. In addition to *ortho*- and *ortho-peri*-extension in **2a**−**2d** and **3a** and **3b**, we present *peri*-fusion by formally adding phenalene units to indeno[1,2-*b*]fluorene.

The targeted IDPs **1a** and **1b** were synthesized starting from 4,4,5,5-tetramethyl-2-pyren-2-yl-[1,3,2]dioxaborolane (**4a**) or 2-(7-*tert*-butylpyren-2-yl)-4,4,5,5-tetramethyl-[1,3,2]-dioxaborolane (**4b**), which were both easily accessible by the C−H borylation of pyrene developed by the group of Marder (Scheme 1).[23] The Suzuki reaction of **4a** and **4b** and 2,5-dibromoterephthalaldehyde[24] provided linear 2,5-di(pyren-2-yl)terephthalaldehyde (**5a**) and 2,5-bis(7-(*tert*-butyl)pyren-2-yl)terephthalaldehyde (**5b**). The crude compounds **5a** and **5b** were suspended in THF and treated with mesityl magnesium bromide. Without further purification, a Friedel−Crafts reaction induced by boron trifluoride diethyl etherate afforded the highly blue fluorescent precursor molecules, 8,18-dimesityl-8,18-dihydro-*s*-indaceno[2,1-*a*:6,5-*a*′]dipyrene (**6a**) and 2,12-di-*tert*-butyl-8,18-dimesityl-8,18-dihydro-*s*-indaceno[2,1-*a*:6,5-*a*′]dipyrene (**6b**) in a yield of 90% and 86% over two steps, respectively. In the final step, treatment of **6a** and **6b** with 2,3-dichloro-5,6-dicyano-1,4-benzoquinone (DDQ) in dry toluene afforded the desired products **1a** and **1b** as green solids in yields of 69% and 60%, respectively, after filtration over aluminum oxide and subsequent precipitation in methanol. Both targeted compounds showed reasonable solubility (1.3 mgmL^{-1}) in toluene and tetrachloroethane. Two-dimensional NMR spectroscopy (^{1}H/^{1}H−COSY/NOESY, see Supporting Information, Figures S9−S12 and S16−S17) allowed a full proton assignment of **1a** and **1b** after the addition of hydrazine to remove trace radical impurities.[25]

Single crystals of **1a** and **1b** suitable for X-ray analysis were obtained by slow evaporation of their solutions in a CS_2/*n*-hexane mixture, and their molecular arrangements were unambiguously confirmed. Both compounds **1a** (Figure 2) and **1b** (Supporting Information, Figure S18) possess a planar π-conjugated carbon skeleton and a C_2 point symmetry. The

Scheme 1. Synthesis of 1a and 1b

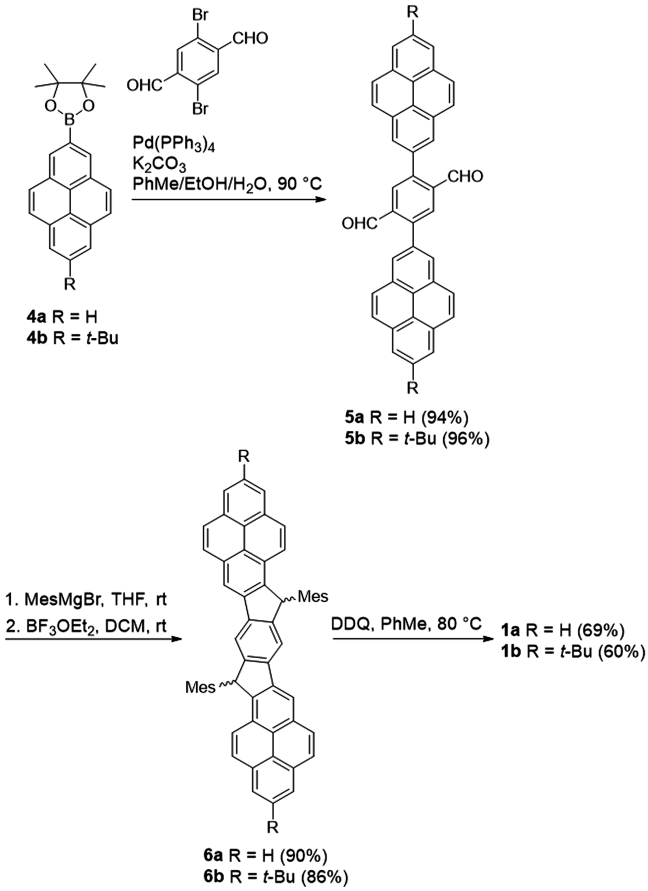

central core possesses two short C(sp^2)−C(sp^2) bonds (1.356(2) and 1.357(2) Å for **1a** and **1b**) and four long C(sp^2)−C(sp^2) bonds (1.425(2)/1.457(2) Å for **1a** and 1.432(2)/1.452(2) Å for **1b**). These bond lengths are in agreement with known *p*-quinoidal substructures.[18,22]

To investigate the optoelectronic properties, UV/vis absorption spectra of solutions of **1a** and **1b** in DCM were recorded and are shown in Figure 3a. The absorption of **1a** and **1b** is strongly red-shifted compared to the parent IF, and broad absorptions between 500 and 800 nm with local maxima at 630 and 634 nm as well as global maxima at 676 and 682 nm, respectively, are found. No fluorescence was detected when excited with UV light, as expected for PHs with an antiaromatic character.[26]

The redox properties of **1a** and **1b** were investigated by cyclic voltammetry (CV) measurements (Figure 3b). IDP **1a** shows two reversible oxidation waves with half wave potentials $E_{1/2,ox}$ at 0.76 and 1.03 V and two reversible reduction waves with half-wave potentials $E_{1/2,red}$ at −0.86 and −1.24 V (vs Ag/AgCl). Two reversible oxidation waves with $E_{1/2,ox}$ at 0.72 and 0.97 V and two reversible reduction waves with $E_{1/2,red}$ at −0.88 and −1.28 V were observed for compound **1b**. Thus, the HOMO/LUMO energy levels are estimated to be −5.02/−3.44 eV and −5.00/−3.40 eV for **1a** and **1b**, respectively, on the basis of the onset potentials of the first oxidation/reduction waves.

The corresponding, electrochemical-derived energy gaps (ΔE_g) are 1.58 and 1.60 eV for **1a** and **1b**, respectively, which are in agreement with their calculated optical energy gaps (Table 1). Compared to the reported 6,12-dimesitylindeno[1,2-*b*]fluorene (ΔE_g = 2.22 eV),[14] the energy gap decreased by 0.6

DOI: 10.1021/acs.joc.8b00925
J. Org. Chem. 2018, 83, 6633−6639

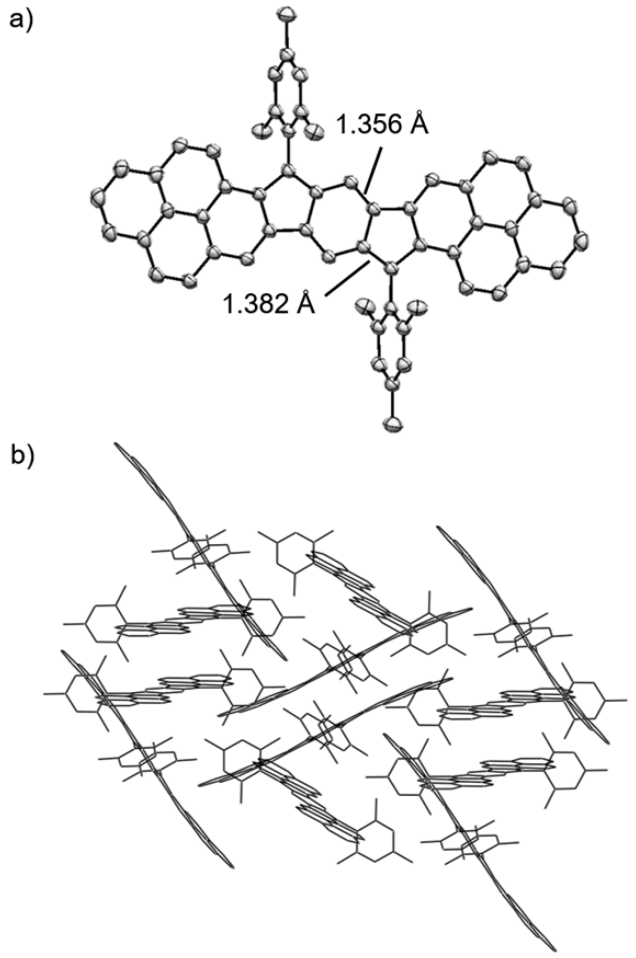

Figure 2. Molecular structure (a) and packing in solid state (b) of **1a**; hydrogen atoms are omitted for clarity, and the thermal ellipsoids are displayed at a 50% probability.

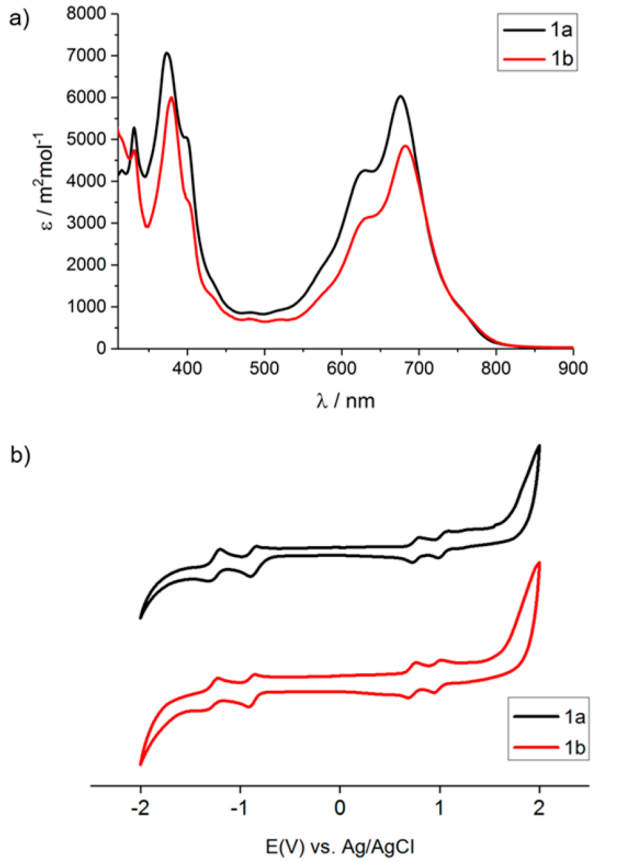

Figure 3. (a) UV/vis absorption spectra of **1a** (black line) and **1b** (red line) in DCM at 10^{-5} molL^{-1}. (b) Cyclic voltamograms of **1a** (black line) and **1b** (red line) in a potential range of −2 to 2 V in dry DCM with 0.1 M *n*-BuNPF$_6$ as the supporting electrolyte, Ag/AgCl was used as a reference electrode, platinum as a working electrode, and a Pt-wire as a counter electrode performed at a scan rate of 50 mVs^{-1}.

eV as the HOMO energy increased from −5.78 eV up to −5.02 and −5.00 eV, for **1a** and **1b**, respectively.[22] The LUMO energy increased from −3.56 eV for the parent IF to −3.44 and −3.40 eV for **1a** and **1b**, respectively.

The reversible oxidation found for **1a** and **1b** encouraged us to investigate the generation of the cation radical and dicationic species. First, UV/vis oxidation titration of both solutions in anhydrous dichloromethane (DCM) was performed with the one-electron-oxidant $AgSbF_6$.

The addition of 1.0−2.0 equiv (eq) of $AgSbF_6$ to the solution of **1a** induced a strong bathochromic shift of the maximum absorption to 1007 nm, and minor absorptions arose between 1050 and 1700 nm with local maxima at 1113, 1271, and 1452 nm, as exemplified in Figure 4a for **1a** (see Supporting Information, Figure S20a for **1b**). These absorptions can be attributed to the formation of radical cations $\mathbf{1a}^{\bullet+}$, most likely paired with SbF_6^- as the counterion. After the addition of 4.5 equiv of $AgSbF_6$, the initial IDP **1a** was completely converted, according to the vanished absorptions between 600 and 800 nm. Upon further addition of an excess of 40 equiv of $AgSbF_6$, a hypsochromic shift to 858 nm (Figure 4b, see Supporting Information, Figure S20b for **1b**) was observed, which we interpret as the formation of a dication $\mathbf{1a}^{2+}$. No further changes of the UV/vis absorption spectra were detected after the addition of more than 50 equiv of $AgSbF_6$ for both compounds.

Density functional theory (DFT) and time-dependent DFT (TD-DFT) calculation were performed using the Gaussian 09 package. The geometry of all of the structures were optimized at the B3LYP level of theory with the 6-31G(d) basis set. The TD-DFT calculation was performed on the neutral, radical cation and dication compounds in order to study the excited states. The graphical representation of the calculated UV/vis spectra for **1a**, $\mathbf{1a}^{\bullet+}$, $\mathbf{1a}^{2+}$, **1b**, $\mathbf{1b}^{\bullet+}$, and $\mathbf{1b}^{2+}$ and the shapes of the frontier orbital, as well as the values for neutral structures in vacuo calculated by the Gaussian 09 package, are summarized in the Supporting Information (Figures S30−S35).

The HOMO and LUMO orbitals are mainly distributed around the *s*-indacene core as well as at the margin areas of the pyrene scaffold for both compounds **1a** and **1b**, as pictured in Figure 5 for **1a** (see Supporting Information, Figures S25−S27 for **1b**). The DFT calculated energy gaps for **1a** and **1b** are 1.77 eV. These results are in agreement with the experimental data and are summarized together in Table 1. The calculated energy gaps are located in between the experimental UV/vis and electrochemical results and closer to the optical derived values of 1.84 and 1.82 eV for **1a** and **1b**, respectively. The differences in the energy gaps derived by the calculation, absorption spectroscopy, and CV may arise from the polarization effects during the measurement in DCM.

DOI: 10.1021/acs.joc.8b00925
J. Org. Chem. 2018, 83, 6633−6639

Table 1. Experimental and Calculated Values of Optoelectronic Data

	UV/vis		electrochemistry			DFT calculations		
compd	λ_{max} [a] (nm)	opt. ΔE_g [b] (eV)	E_{HOMO} [c] (eV)	E_{LUMO} [d] (eV)	ΔE_g [e] (eV)	E_{HOMO} [f] (eV)	E_{LUMO} [g] (eV)	ΔE_g [h] (eV)
1a	676	1.84	−5.02	−3.44	1.58	−4.57	−2.79	1.77
1b	682	1.82	−5.00	−3.40	1.60	−4.51	−2.74	1.77

[a]Absorption at maximum wavelength. [b]Optical energy gap calculated from the UV/vis absorption maxima using the Planck-Einstein relation. [c]HOMO estimated from the onset potential of the first oxidation wave. [d]LUMO estimated from the onset potential of the first reduction wave. [e]Energy gap calculated according to $\Delta E_g = E_{HOMO} - E_{LUMO}$. [f]HOMO calculated by DFT Gaussian 09 package. [g]LUMO calculated by DFT Gaussian 09 package. [h]Energy gap calculated according to $\Delta E_g = E_{HOMO} - E_{LUMO}$.

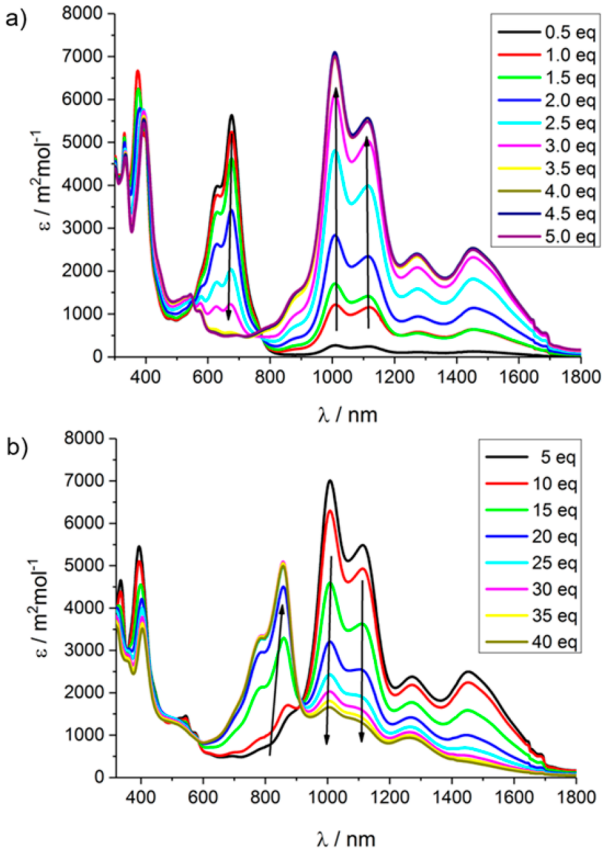

Figure 4. UV/vis absorption titration spectra using a solution of a one-electron-oxidant $AgSbF_6$ in dry DCM at 10^{-5} molL^{-1}. UV/vis spectra were directly measured after the addition of the oxidant. (a) UV/vis absorption during the titration of **1a** into **1a**$^{\bullet+}$ by adding 0−4.5 equiv of oxidant in steps of 0.5 equiv. (b) UV/vis absorption during the titration of **1a**$^{\bullet+}$ to **1a**$^{2+}$ by further adding up to 40 equiv of $AgSbF_6$.

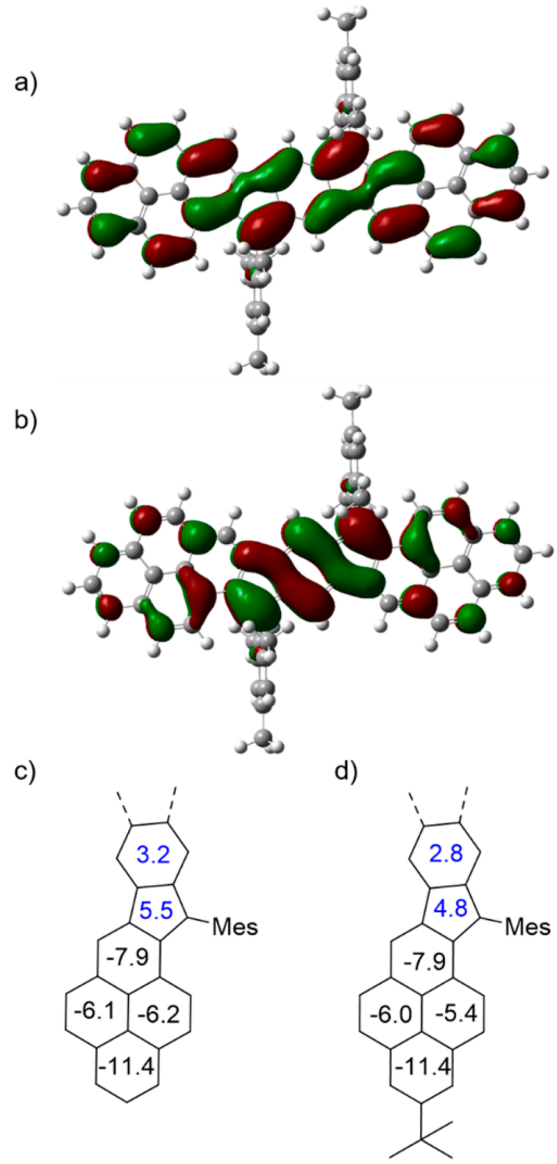

Figure 5. Visualization of the frontier orbitals and NICS calculation. (a) HOMO **1a** (−4.57 eV); (b) LUMO **1a** (−2.79 eV); (c) NICS(1) values of **1a**; and (d) NICS(1) values of **1b**.

To verify the antiaromatic feature at the internal *s*-indacene core, NICS(1) calculations using the GIAO B3LYP/6-311+G-(2d,p) method have been performed.

For **1a** and **1b**, NICS values are positive at the five-membered (5.5 and 4.8, respectively) and central six-membered (3.2 and 2.8, respectively) rings, confirming the preserved antiaromaticity of the *s*-indacene unit (Figure 5c,d). The negative values for the outer pyrene units are in accordance with calculations by Jenneskens and confirm the proposed structure and electronic character of pyrene-fused *s*-indacene.[27]

CONCLUSION

In summary, we present two novel antiaromatic *s*-indacenodipyrenes (IDPs) with a large bathochromic shift compared to that of the parent IF and its derivatives. Photophysical and electrochemical measurements demonstrated that IDPs **1a** and **1b** possess absorption maxima approaching the NIR region combined with excellent redox behavior. The simple and scalable synthetic protocols toward antiaromatic PHs by combining two pyrene scaffolds with a functionalized benzene core enables the extension toward stable and π-expanded ladder-type polymers representing a repeating IF motive.

DOI: 10.1021/acs.joc.8b00925
J. Org. Chem. 2018, 83, 6633−6639

EXPERIMENTAL SECTION

General Methods. Unless otherwise stated, commercially available starting materials, catalysts, reagents, and dry solvents were used without further purification. Reactions were performed using standard vacuum-line and Schlenk techniques. Purification of **4a**, **4b**, **5a**, and **5b** was carried out under ambient conditions using reagent-grade solvents. Purification of **1a** and **1b** was carried out under argon conditions using dry and bubbled toluene and methanol. Column chromatography was performed on silica (SiO_2, particle size 0.063−0.200 mm, purchased from VWR) or aluminum oxide (Al_2O_3, Alox 90 active neutral, activity stage I, purchased from Merck KGaA). Silica-coated aluminum sheets with a fluorescence indicator (TLC silica gel 60 F_{254}, purchased from Merck KGaA) were used for thin layer chromatography. The starting materials **4a**, **4b**,[1] and 2,5-dibromoterephthalaldehyde[2] were synthesized according to literature procedures. MALDI-TOF-HRMS spectra were recorded on a Bruker Autoflex Speed MALDI-TOF MS (Bruker Daltonics, Bremen, Germany). All of the samples were prepared by mixing the analyte and the matrix, 1,8-dihydroxyanthracen-9(10*H*)-one (dithranol, purchased from Fluka Analytical, purity >98%), in the solid state. NMR data were recorded on a Bruker AV-II 300 spectrometer operating at 300 MHz for ^{1}H and 75 MHz for ^{13}C and on a Bruker AV-III 600 spectrometer operating at 600 MHz for ^{1}H and 151 MHz for ^{13}C with standard Bruker pulse programs at room temperature (296 K). Chemical shifts were referenced to δ_{TMS} = 0.00 ppm (^{1}H, ^{13}C). Chemical shifts (δ) are reported in ppm. Coupling constants (J) are reported in Hz. Dichloromethane-d_2 (δ (^{1}H) = 5.32 ppm, δ (^{13}C) = 53.8 ppm), tetrachloroethane-d_2 (δ (^{1}H) = 5.91 ppm, δ (^{13}C) = 74.2 ppm), or chloroform-d_1 (δ (^{1}H) = 7.26 ppm, δ (^{13}C) = 77.16 ppm) were used as solvents. The following abbreviations are used to describe peak patterns as appropriate: s = singlet, d = doublet, t = triplet, q = quartet, and m = multiplet. Dichloromethane-d_2 (99.9 atom% D) was purchased from Euriso-top, tetrachloroethane-d_2 (99.6 atom% D) was purchased from Carl Roth GmbH, and chloroform-d_1 (99.8 atom% D) was purchased from Deutero GmbH. UV/vis−NIR absorption spectroscopy was conducted on an Agilent Technologies Cary Series 5000 using a 10 mm optical-path quartz cell at room temperature. Unless otherwise stated, a solution of the target compounds at a concentration of 10^{-5} molL^{-1} in dichloromethane was measured. Fluorescence spectra were recorded at room temperature on a PerkinElmer Fluorescence Spectrometer LS 55 using a 10 mm fluorescence quartz cell and argon-purged solutions of the respective compounds (10^{-5} molL^{-1} in anhydrous dichloromethane). Cyclic voltammetry measurements were carried out on a CHI 760 E potentiostat (CH Instruments) in a three-electrode cell. Electrolyte solutions were prepared by dissolving [nBu$_4$N][PF$_6$] 0.1 M in dichloromethane, and the experiments were performed with a scan rate of 50 mVs^{-1} at room temperature. All measurements were recorded in argon-purged solutions of **1a** and **1b** in anhydrous dichloromethane. A Pt-electrode and a Pt-wire were used as a working and counter electrode, respectively. Ag/AgCl (3 M KCl solution) was used as a reference electrode. All electrochemical measurements were referenced by adding an adequate amount of Cp_2Fe. The oxidation potential for ferrocene $E_{1/2}$(Cp_2Fe/Cp_2Fe^+) in dichloromethane was observed at 0.44 eV. Melting points were determined on a Büchi Melting Point M-560 in a range of 50−400 °C with a temperature rate of 10 °C min^{-1}. Density functional theory (DFT) and time-dependent DFT (TD-DFT) calculations were performed using the Gaussian 09 rev. A02 package.[3] The geometry of all of the structures was optimized at the B3LYP level of theory with the 6-31G(d) basis set. The TD-DFT calculation has been performed on the neutral, radical cation and dication compounds in order to study the excited states.

Preparation of *s*-Indacenodipyrenes 1a and 1b. *2,5-Di(pyren-2-yl)terephthalaldehyde (**5a**).* 2,5-Dibromoterephthalaldehyde (162 mg, 0.55 mmol, 1.0 equiv), **4a** (546 mg, 1.66 mmol, 3.0 equiv), and K_2CO_3 (460 mg, 3.33 mmol, 6.0 equiv) were added to a mixture of toluene (9 mL), ethanol (3 mL), and water (3 mL) in a 25 mL Schlenk flask and purged for 30 min with argon. After the addition of $Pd(PPh_3)_4$ (128 mg, 0.11 mmol, 0.2 equiv) as catalyst, the reaction mixture was stirred under reflux at 90 °C for 20 h in an oil bath. The reaction mixture was allowed to cool to room temperature, and water (50 mL) as well as chloroform (100 mL) were added. The organic phase was collected, and all volatiles were removed under reduced pressure. The remaining solid was suspended in methanol and filtered to give the crude precursor **5a** as a yellow powder (94%, 278 mg, 0.52 mmol), which was used without further purification. Due to the extreme low solubility of **5a** in common NMR solvents, such as deuterated dichloromethane-d_2, chloroform-d_1, tetrachloroethane-d_2, tetrahydrofuran-d_4, toluene-d_8, or chlorobenzene-d_5, a detailed spectroscopic NMR investigation was not possible. The precursor **5a** was confirmed by high-resolution mass spectrometry. MALDI-TOF-HRMS (m/z): calculated for $C_{40}H_{22}O_2$, 534.1630; found, 534.1620, error = +1.87 ppm.

*2,5-Bis(7-(tert-butyl)pyren-2-yl)terephthalaldehyde (**5b**).* 2,5-Dibromoterephthalaldehyde (50 mg, 0.17 mmol, 1.0 equiv), **4b** (197 mg, 0.51 mmol, 3.0 equiv), and K_2CO_3 (142 mg, 1.03 mmol, 6.0 equiv) were added to a mixture of toluene (3 mL), ethanol (1 mL), and water (1 mL) in a 10 mL Schlenk flask and purged for 30 min with argon. After the addition of the catalyst $Pd(PPh_3)_4$ (39 mg, 0.03 mmol, 0.2 equiv), the reaction mixture was heated under reflux at 90 °C for 20 h in an oil bath. After cooling down to room temperature, the reaction was quenched by adding water (100 mL). The aqueous phase was extracted three times with chloroform (100 mL). The combined organic layers were dried over $MgSO_4$, filtered, and all volatiles were evaporated under reduced pressure. The remaining solid was suspended in methanol and filtered to yield precursor **5b** as pale green powder (96%, 105 mg, 0.16 mmol), which was used without further purification. ^{1}H NMR (300 MHz, tetrachloroethane-d_2, δ): 10.12 (s, 2H), 8.37 (s, 2H), 8.25 (s, 4H), 8.21 (s, 4H), 8.14 (d, J = 9.0 Hz, 4H), 8.08 (d, J = 9.0 Hz, 4H), 1.54 (s, 18H) ppm. ^{13}C NMR (75 MHz, tetrachloroethane-d_2, δ): 192.6, 150.3, 145.4, 137.0, 133.8, 131.4, 131.3, 129.3, 127.4, 126.4, 124.5, 123.4, 122.6, 35.6, 32.2 ppm. MALDI-TOF-HRMS (m/z): calculated for $C_{48}H_{38}O_2$, 646.2892; found, 646.2872, error = +3.09 ppm.

*8,18-Dimesityl-*s*-indaceno[2,1-a:6,5-a′]dipyrene (**1a**).* Precursor **5a** (250 mg, 0.47 mmol, 1.0 equiv) was dissolved in 150 mL of tetrahydrofuran (THF) in a dry Schlenk flask, and a solution of 2-mesityl magnesium bromide in THF (7.0 mL, 1.0 M, 7.00 mmol, 15.0 equiv) was added slowly at room temperature. The mixture was stirred overnight, quenched by the slow addition of water (100 mL), and the aqueous phase was extracted three times with chloroform (100 mL) afterward. The combined organic layers were dried over $MgSO_4$, filtered, and all volatiles were evaporated under reduced pressure. The crude material was then transferred to a dry 50 mL Schlenk flask and dissolved in 30 mL of dichloromethane. The mixture was cooled down to 0 °C, and a solution of boron trifluoride diethyl etherate (230 μL, 1.87 mmol, 4.0 equiv) was added slowly in the course of 5 min. The mixture was stirred for 1 h and was carefully quenched with a saturated $NaHCO_3$ solution (10 mL) afterward. The aqueous phase was extracted three times with chloroform (50 mL). The combined organic phases were again dried over $MgSO_4$, filtered, and all volatiles were removed under reduced pressure. The obtained residue was filtered over a short silica plug (chloroform/*iso*-hexane: 1:4) to result in an isomeric mixture of intermediated **6a** (see Scheme 1) as light green solid. Intermediate **6a** (20 mg, 0.027 mmol, 1.0 equiv) and 2,3-dichloro-5,6-dicyano-1,4-benzoquinone (DDQ, 12 mg, 0.055 mmol, 2.0 equiv) were redissolved in toluene (3 mL) in a dry 10 mL Schlenk flask, and the mixture was heated at 80 °C in an oil bath. After 2 h, the reaction mixture was allowed to cool down to room temperature. Due to its low stability, the solution was quickly filtered through an aluminum oxide (neutral) column with dry toluene as an eluent under an argon atmosphere. All volatiles were evaporated under reduced pressure, the remaining solid was suspended in dry and argon-purged methanol and filtered to yield the blue-greenish target compound **1a** in a good yield (69%, 14 mg, 0.019 mmol). The intermediate **6a** was confirmed by MALDI-TOF-HRMS ((m/z): calculated for $C_{58}H_{42}$, 738.3281; found, 738.3287, error = 0.81 ppm). Due to the bad solubility (1.3 mgml^{-1}) of **1a** the ^{13}C NMR measurements only show a low resolution. Full analytical data of target compound **1a**: ^{1}H NMR (600 MHz, tetrachloroethane-d_2, after addition of hydrazine, δ): 8.02

DOI: 10.1021/acs.joc.8b00925
J. Org. Chem. 2018, 83, 6633−6639

(s, 2H), 7.91 (d, J = 7.4 Hz, 2H), 7.83−7.79 (m, 4H), 7.77 (d, J = 8.9 Hz, 2H), 7.72 (t, J = 7.5 Hz, 2H), 7.56 (d, J = 9.4 Hz, 2H), 7.20 (d, J = 9.3 Hz, 2H), 7.07 (s, 4H), 7.04 (s, 2H), 2.44 (s, 6H), 2.18 (s, 12H) ppm. ^{13}C NMR (151 MHz, tetrachloroethane-d_2, after addition of hydrazine, δ): 147.1, 138.9, 138.0, 137.7, 137.3, 137.2, 137.0, 132.8, 132.0, 131.4, 131.2, 128.8 (4 CH), 128.7 (2 CH), 128.6 (2 CH), 127.7 (2 CH), 127.6, 126.3 (2 CH), 125.9 (2 CH), 125.5 (2 CH), 123.8, 122.8 (2 CH), 119.2 (2 CH), 118.5 (2 CH), 117.1, 116.9, 116.7, 21.8 (2 CH_3), 20.8 (4 CH_3) ppm. HRMS-MALDI-TOF (m/z): calculated for $C_{58}H_{40}$, 736.3130; found, 736.3130, error = ± 0 ppm. mp > 400 °C.

*2,12-Ditert-butyl-8,18-dimesityl-s-indaceno[2,1-a:6,5-a′]dipyrene (**1b**).* Precursor **5b** (100 mg, 0.17 mmol, 1.0 equiv) was dissolved in 50 mL of THF in a dry Schlenk flask, and a solution of 2-mesityl magnesium bromide in THF (2.6 mL, 1.0 M, 2.55 mmol, 15.0 equiv) was added slowly at room temperature. The mixture was stirred overnight and quenched afterward by a slow addition of water (50 mL). The aqueous phase was extracted three times with chloroform (50 mL). The combined organic layers were dried over $MgSO_4$, filtered, and all volatiles were evaporated under reduced pressure. The crude material was transferred to a dry 50 mL Schlenk flask and dissolved in 20 mL of dichloromethane. The mixture was cooled down to 0 °C, and a solution of boron trifluoride diethyl etherate (85 μL, 0.68 mmol, 4.0 equiv) was added slowly in the course of 5 min. The mixture was stirred for 1 h and was carefully quenched by the addition of a saturated $NaHCO_3$ solution (5 mL) afterward. The aqueous phase was extracted three times with chloroform (50 mL), and the resulting combined organic phases were dried over $MgSO_4$, filtered, and all volatiles were removed under reduced pressure. The obtained residue was filtered over a short silica plug (chloroform/*i*-hexane, 1:4) to give an isomeric mixture of intermediate **6b** (see Scheme 1) as light green solid. **6b** (12 mg, 0.014 mmol, 1.0 equiv) and 2,3-dichloro-5,6-dicyano-1,4-benzoquinone (DDQ, 6 mg, 0.027 mmol, 2.0 equiv) were dissolved in toluene (2 mL) in a dry 10 mL Schlenk flask, and the mixture was heated at 80 °C in an oil bath. After 2 h, the reaction mixture was allowed to cool down to room temperature. Due to its low stability, the solution was quickly filtered through an aluminum oxide (neutral) column with dry toluene as an eluent under an argon atmosphere. All volatiles were evaporated under reduced pressure, the remaining solid was suspended in dry and argon-purged methanol and filtered to give the blue-greenish target compound **1b** in a good yield (60%, 7 mg, 0.082 mmol). The intermediate **6b** was confirmed by MALDI-TOF-HRMS ((m/z): calculated for $C_{66}H_{58}$, 850.4593; found, 850.4539, error = 6.35 ppm). Due to the bad solubility (1.3 mgmL^{-1}) of **1b**, the ^{13}C NMR measurements only show a low resolution. Full analytical data of target compound **1b**: ^{1}H NMR (600 MHz, tetrachloroethane-d_2, after addition of hydrazine, δ): 7.97 (s, 2H), 7.92 (d, J = 1.6 Hz, 2H), 7.82 (d, J = 1.6 Hz, 2H), 7.78 (d, J = 9.0 Hz, 2H), 7.74 (d, J = 9.0 Hz, 2H), 7.53 (d, J = 9.5 Hz, 2H), 7.15 (d, J = 9.2 Hz, 2H), 7.07 (s, 4H), 7.01 (s, 2H), 2.44 (s, 6H), 2.17 (s, 12H), 1.41 (s, 18H) ppm. ^{13}C NMR (151 MHz, tetrachloroethane-d_2, after addition of hydrazine, δ): 149.4 (2C), 147.0 (2C), 139.0 (2C), 138.0 (2C), 137.6 (2C), 137.2 (2C), 137.0 (2C), 132.8 (2C), 131.9 (2C), 131.2 (2C), 131.0 (2C), 128.9 (2CH), 128.7 (2CH), 128.5 (2CH), 127.9 (2CH), 127.4 (2C), 125.9 (2C), 124.1 (2C), 123.8 (2C), 123.1 (2CH), 122.9 (2CH), 122.7 (2CH), 119.0 (2CH), 118.3 (2CH), 116.9 (2C), 35.2 (2C), 32.0 (6CH_3), 21.8 (2CH_3), 20.8 (4CH_3) ppm. MALDI-TOF-HRMS (m/z): calculated for $C_{66}H_{56}$, 848.4393; found, 848.4382, error = +1.30 ppm. mp > 400 °C.

■ ASSOCIATED CONTENT

Supporting Information

The Supporting Information is available free of charge on the ACS Publications website at DOI: 10.1021/acs.joc.8b00925.

HR-MALDI-TOF spectra for **1a** and **1b**; copies of the ^{1}H-and ^{13}C NMR spectra for **5a**, **5b**, **1a**, and **1b**; single-crystal X-ray data for **1a** and **1b**; UV/vis absorption spectra for **1a**, **1a**$^{\bullet+}$, **1a**$^{2+}$, **1b**, **1b**$^{\bullet+}$, and **1b**$^{2+}$; fluorescence emission spectra and cyclic voltamograms for **1a** and **1b**; and computational data for **1a**, **1a**$^{\bullet+}$, **1a**$^{2+}$, **1b**, **1b**$^{\bullet+}$, and **1b**$^{2+}$ (PDF)

X-ray crystallographic data for compound **1a** (CIF)

X-ray crystallographic data for compound **1b** (CIF)

■ AUTHOR INFORMATION

Corresponding Authors

*E-mail: reinhard.berger@tu-dresden.de.

*E-mail: xinliang.feng@tu-dresden.de.

ORCID

Junzhi Liu: 0000-0001-7146-0942

Jan J. Weigand: 0000-0001-7323-7816

Reinhard Berger: 0000-0002-8959-7821

Xinliang Feng: 0000-0003-3885-2703

Notes

The authors declare no competing financial interest.

■ ACKNOWLEDGMENTS

This project has received funding from the European Union's Horizon 2020 research and innovation program under grant agreement 696656 (Graphene Flagship Core1), the Center for Advancing Electronics Dresden (cfaed), the European Social Fund, and the Federal State of Saxony (ESF-Project "GRAPHD", TU Dresden). We thank Dr. Tilo Lübken (Dresden University of Technology) for NMR measurements. Prof. Dr. Jan J. Weigand thanks the DFG for funding a diffractometer (INST 269/618-1).

■ REFERENCES

(1) Zeng, Z.; Shi, X.; Chi, C.; Lopez Navarrete, J. T.; Casado, J.; Wu, J. Pro-aromatic and anti-aromatic π-conjugated molecules: an irresistible wish to be diradicals. *Chem. Soc. Rev.* **2015**, *44*, 6578−6596.

(2) Chase, D. T.; Rose, B. D.; McClintock, S. P.; Zakharov, L. N.; Haley, M. M. Indeno[1,2-*b*]fluorenes: fully conjugated antiaromatic analogues of acenes. *Angew. Chem., Int. Ed.* **2011**, *50*, 1127−1130.

(3) Sun, Z.; Zeng, Z.; Wu, J. Zethrenes, extended *p*-quinodimethanes, and periacenes with a singlet biradical ground state. *Acc. Chem. Res.* **2014**, *47*, 2582−2591.

(4) Nishinaga, T.; Ohmae, T.; Aita, K.; Takase, M.; Iyoda, M.; Arai, T.; Kunugi, Y. Antiaromatic planar cyclooctatetraene: a strategy for developing ambipolar semiconductors for field effect transistors. *Chem. Commun.* **2013**, *49*, 5354−5356.

(5) Das, A.; Müller, T.; Plasser, F.; Lischka, H. Polyradical Character of Triangular Non-Kekulé Structures, Zethrenes, *p*-Quinodimethane-Linked Bisphenalenyl, and the Clar Goblet in Comparison: An Extended Multireference Study. *J. Phys. Chem. A* **2016**, *120*, 1625−1636.

(6) Das, S.; Wu, J. Polycyclic Hydrocarbons with an Open-Shell Ground State. In *Chemistry of Carbon Nanostructures*; Müllen, K., Feng, X.; Walter de Gruyter GmbH: Berlin, 2017; pp 253−288.

(7) Shimizu, A.; Tobe, Y. Indeno[2,1-*a*]fluorene: An Air-Stable *ortho*-Quinodimethane Derivative. *Angew. Chem., Int. Ed.* **2011**, *50*, 6906−6910.

(8) Li, Y.; Huang, K.-W.; Sun, Z.; Webster, R. D.; Zeng, Z.; Zeng, W.; Chi, C.; Furukawa, K.; Wu, J. A kinetically blocked 1,14:11,12-dibenzopentacene: a persistent triplet diradical of a non-Kekulé polycyclic benzenoid hydrocarbon. *Chem. Sci.* **2014**, *5*, 1908−1914.

(9) Das, S.; Lee, S.; Son, M.; Zhu, X.; Zhang, W.; Zheng, B.; Hu, P.; Zeng, Z.; Sun, Z.; Zeng, W.; Li, R.-W.; Huang, K.-W.; Ding, J.; Kim, D.; Wu, J. *para*-Quinodimethane-Bridged Perylene Dimers and Pericondensed Quaterrylenes: The Effect of the Fusion Mode on the Ground States and Physical Properties. *Chem. - Eur. J.* **2014**, *20*, 11410−11420.

DOI: 10.1021/acs.joc.8b00925
J. Org. Chem. 2018, 83, 6633−6639

(10) Ohashi, K.; Kubo, T.; Masui, T.; Yamamoto, K.; Nakasuji, K.; Takui, T.; Kai, Y.; Murata, I. 4,8,12,16-Tetra-*tert*-butyl-*s*-indaceno[1,2,3-*cd*:5,6,7-*c*′*d*′]diphenalene: A Four-Stage Amphoteric Redox System. *J. Am. Chem. Soc.* **1998**, *120*, 2018−2027.
(11) Li, Y.; Heng, W. K.; Lee, B. S.; Aratani, N.; Zafra, J. L.; Bao, N.; Lee, R.; Sung, Y. M.; Sun, Z.; Huang, K. W.; Webster, R. D.; Lopez Navarrete, J. T.; Kim, D.; Osuka, A.; Casado, J.; Ding, J.; Wu, J. Kinetically blocked stable heptazethrene and octazethrene: closed-shell or open-shell in the ground state? *J. Am. Chem. Soc.* **2012**, *134*, 14913−14922.
(12) Shimizu, A.; Hirao, Y.; Matsumoto, K.; Kurata, H.; Kubo, T.; Uruichi, M.; Yakushi, K. Aromaticity π-bond covalency: prominent intermolecular covalent bonding interaction of a Kekulé hydrocarbon with very significant singlet biradical character. *Chem. Commun.* **2012**, *48*, 5629−5631.
(13) Tobe, Y. Quinodimethanes Incorporated in Non-Benzenoid Aromatic or Antiaromatic Frameworks. *Top. Curr. Chem.* **2018**, *376*, 12.
(14) Chase, D. T.; Fix, A. G.; Kang, S. J.; Rose, B. D.; Weber, C. D.; Zhong, Y.; Zakharov, L. N.; Lonergan, M. C.; Nuckolls, C.; Haley, M. M. 6,12-Diarylindeno[1,2-*b*]fluorenes: Syntheses, Photophysics, and Ambipolar OFETs. *J. Am. Chem. Soc.* **2012**, *134*, 10349−10352.
(15) Anthony, J. E. The larger acenes: versatile organic semiconductors. *Angew. Chem., Int. Ed.* **2008**, *47*, 452−483.
(16) Anthony, J. E. Functionalized Acenes and Heteroacenes for Organic Electronics. *Chem. Rev.* **2006**, *106*, 5028−5048.
(17) Wu, J.; Pisula, W.; Müllen, K. Graphenes as Potential Material for Electronics. *Chem. Rev.* **2007**, *107*, 718−747.
(18) Frederickson, C. K.; Zakharov, L. N.; Haley, M. M. Modulating Paratropicity Strength in Diareno-Fused Antiaromatics. *J. Am. Chem. Soc.* **2016**, *138*, 16827−16838.
(19) Petersen, J. F.; Frederickson, C. K.; Marshall, J. L.; Rudebusch, G. E.; Zakharov, L. N.; Hammerich, O.; Haley, M. M.; Nielsen, M. B. Expanded Indacene−Tetrathiafulvalene Scaffolds: Structural Implications for Redox Properties and Association Behavior. *Chem. - Eur. J.* **2017**, *23*, 13120−13130.
(20) Marshall, J. L.; Uchida, K.; Frederickson, C. K.; Schutt, C.; Zeidell, A. M.; Goetz, K. P.; Finn, T. W.; Jarolimek, K.; Zakharov, L. N.; Risko, C.; Herges, R.; Jurchescu, O. D.; Haley, M. M. Indacenodibenzothiophenes: synthesis, optoelectronic properties and materials applications of molecules with strong antiaromatic character. *Chem. Sci.* **2016**, *7*, 5547−5558.
(21) Marshall, J. L.; O'Neal, N. J.; Zakharov, L. N.; Haley, M. M. Synthesis and Characterization of Two Unsymmetrical Indenofluorene Analogues: Benzo[5,6]-*s*-indaceno[1,2-*b*]thiophene and Benzo[5,6]-*s*-indaceno[2,1-*b*]thiophene. *J. Org. Chem.* **2016**, *81*, 3674−3680.
(22) Liu, J.; Ma, J.; Zhang, K.; Ravat, P.; Machata, P.; Avdoshenko, S.; Hennersdorf, F.; Komber, H.; Pisula, W.; Weigand, J. J.; Popov, A. A.; Berger, R.; Müllen, K.; Feng, X. π-Extended and Curved Antiaromatic Polycyclic Hydrocarbons. *J. Am. Chem. Soc.* **2017**, *139*, 7513−7521.
(23) Crawford, A. G.; Liu, Z.; Mkhalid, I. A.; Thibault, M. H.; Schwarz, N.; Alcaraz, G.; Steffen, A.; Collings, J. C.; Batsanov, A. S.; Howard, J. A.; Marder, T. B. Synthesis of 2- and 2,7-functionalized pyrene derivatives: an application of selective C-H borylation. *Chem. - Eur. J.* **2012**, *18*, 5022−5035.
(24) Tian, H.; Yang, X.; Chen, R.; Zhang, R.; Hagfeldt, A.; Sun, L. Effect of Different Dye Baths and Dye-Structures on the Performance of Dye-Sensitized Solar Cells Based on Triphenylamine Dyes. *J. Phys. Chem. C* **2008**, *112*, 11023−11033.
(25) Initially solutions of **1a** and **1b** only showed broad signals in the aromatic area (see Supporting Information), which we attribute to the presence of trace amounts of radical impurities arising from immediate oxidation processes.
(26) Frederickson, C. K.; Rose, B. D.; Haley, M. M. Explorations of the Indenofluorenes and Expanded Quinoidal Analogues. *Acc. Chem. Res.* **2017**, *50*, 977−987.
(27) Havenith, R. W. A.; van Lenthe, J. H.; Dijkstra, F.; Jenneskens, L. W. Aromaticity of Pyrene and Its Cyclopentafused Congeners Resonance and NICS Criteria. An Ab Initio Valence Bond Analysis in Terms of Kekulé Resonance Structures. *J. Phys. Chem. A* **2001**, *105*, 3838−3845.

DOI: 10.1021/acs.joc.8b00925
J. Org. Chem. 2018, 83, 6633−6639